J. Biochem. 128, 695–704 (2000)

Conformational Changes in the Unique Loops Bordering the ATP Binding Cleft of Skeletal Muscle Myosin Mediate Energy Transduction[1]

Shinsaku Maruta[2] and Kazuaki Homma

Department of Bioengineering, Faculty of Engineering, Soka University, Hachioji, Tokyo 192-8577

Received June 2, 2000; accepted August 9, 2000

Myosin has three highly-conserved, unique loops [B (320–327), M (677–689), and N (127–136)] at the entrance of the ATP binding cleft, and we previously showed that the effects of actin are mediated by a conformational change in loop M [Maruta and Homma (1998) *J. Biochem.* 124, 528–533]. In the present study, loops M and N were photolabeled respectively with fluorescent probes Mant-8-N_3-ADP and Mant-2-N_3-ADP in order to study conformational changes in the loops related to energy transduction. The effect of actin on the conformation of loop N was examined by analyzing fluorescence polarization and acrylamide quenching; the results were then compared with those previously reported for loop M. In contrast to loop M, the fluorescence polarization and the value of K_{sv} of the Mant-groups crosslinked to loop N were slightly affected by actin binding. To study conformational changes in loops M and N during the ATPase cycle, FRET was analyzed using TNP-ADP·BeFn and TNP-ADP·AlF_4^- as FRET acceptors of Mant fluorescence. The resultant estimated distances between loop M and the active site differed for the Mant-S1·TNP-ADP·BeFn and Mant-S1·TNP-ADP·AlF_4^- complexes, whereas the distances between loop N and the active site differed slightly. These findings indicate that the conformation of loop M changes during the ATPase cycle, suggesting that Loop M acts as a signal transducer mediating communication between the ATP- and actin-binding sites. Loop N, by contrast, is not significantly flexible.

Key words: ATP analogues, energy transduction, fluorescence, myosin, photoaffinity labeling.

Recent crystallographic studies have shown that kinesin (*1*) shows a striking structural similarity to the core of the catalytic domain of myosin (*2–4*), suggesting that these motor proteins share a common mechanism for generating the energy for motility from ATP hydrolysis. On the other hand, myosin has three unique loops—B (aa 320–327), M (aa 677–689), and N (aa 127–136)—in the region of the ATP-binding cleft that are not observed in kinesin; likewise, kinesin contains specific loops L5 and L12. The precise function of these loops is as yet unknown, but they may determine the characteristic properties of motor proteins: *e.g.*, how the interactions between the ATP- and actin-binding sites or between the ATP- and microtubule-binding sites are mediated. Thus, analysis of such loops may be a useful approach to increasing our understanding of the mechanism of energy transduction in motor proteins.

Loop M, which is part of the 20-kDa tryptic fragment of SKE-S1, is unique to myosin and contributes to the structure of the ATP-binding cleft; a key feature of the loop is Lys 681, which actually protrudes into the cleft. Composed primarily of α-helix, the 20-kDa fragment forms the backbone of the myosin head and extends from the actin-binding site to the regulatory region *via* the ATP binding site, and to the hinge area of the reactive cysteine SH1-SH2 region. This arrangement suggests that the 20-kDa fragment and loop M may provide the link through which ATPase activity is modulated by actin.

We previously showed that the fluorescently-labeled, photoreactive, ADP analogue Mant-8-N_3-ADP specifically crosslinks to loop M of skeletal muscle myosin (*5*). Analysis of actin-induced changes in Mant-8-N_3-ADP fluorescence polarization and quenching confirmed that actin binding induces conformational changes in loop M that result in the displacement of Mant-8-N_3-ADP from the ATP-binding cleft, suggesting that loop M may act as a signal transducer mediating communication between the ATP and actin-binding sites (*6*). In addition, loops corresponding to B, N and M were recently shown to be conserved in SMO-S1 (*4*),

[1] This work was supported by Grants-in-Aid for Scientific Research C (11680667) from the Ministry of Education, Science, Sports and Culture of Japan.

[2] To whom correspondence should be addressed. Phone: +81-426-91-9443, Fax: +81-426-91-9312, E-mail: shinsaku@t.soka.ac.jp

Abbreviations: S1, myosin subfragment-1; SKE-S1, skeletal muscle myosin subfragment-1; SMO-S1, smooth muscle myosin subfragment-1; Mant-2-N_3-ADP, 3′-*O*-(*N*-methylanthraniloyl)-2-azido-ADP; Mant-8-N_3-ADP, 3′-*O*-(*N*-methylanthraniloyl)-8-azido-ADP; Mant-2-S1, S1 labeled by Mant-2-N_3-ADP; Mant-8-S1, S1 labeled by Mant-8-N_3-ADP; Mant-S1, S1 labeled by Mant-(2 or 8)-N_3-ADP; AlF_4^-, fluoroaluminate; BeFn, fluoroberyllate; NANDP, 2-[(4-azido-2-nitrophenyl)-amino]ethyl diphosphate; Bz_2-ADP; 3′-*O*-benzoylbenzoic-ADP; Bz_1-εADP, 3′-*O*-benzoylbenzoic-1,N^6-etheno-ADP; FRET, fluorescence resonance energy transfer.

Enzymes: myosin ATPase [EC 3.6.1.32]; trypsin [EC 3.4.21.4]; chymotrypsin [EC 3.4.21.1].

© 2000 by the Japanese Biochemical Society.

Downloaded from http://jb.oxfordjournals.org/ at Peking University on October 1, 2012

and we subsequently found that actin binding induces a conformational change at loop M of SMO-S1 (aa 687–699) (*7*).

Conformational changes in loop N, which contributes to the adenine anchoring site, and loop B, which faces the ribose of ATP, have not been well studied, although analyses of fluorescent polarization by Luo *et al.* (*8*) demonstrated that actin binding has minimal effects on loops N and B of smooth muscle myosin. In the present study, we used fluorescent labeling techniques and fluorescent polarization analysis to assess the effect of actin binding on loop N of SKE-S1 and compared the results with our previously reported data for loop M (*6*). In addition, fluorescence energy transfer spectroscopy was used to analyze the conformational changes in loops M and N during the ATPase cycle in order to assess their potential roles in energy transduction by myosin.

MATERIALS AND METHODS

Protein Preparation—Skeletal muscle myosin was prepared from chicken breast muscle according to the methods of Perry (*9*). The isolated myosin was then digested with α-chymotrypsin to obtain S1 as described by Weeds and Taylor (*10*). F-actin was prepared from chicken skeletal muscle as described by Pardee and Spudich (*11*).

Chemicals—Mant-8-N_3-ATP and Mant-2-N_3-ATP were prepared from 8-N_3-ATP (Sigma) and 2-chloroadenosine (Sigma) as described previously (*5*). $BeSO_4$, $AlCl_3$, and NaF were from Wako Pure Chemical (Tokyo).

Photoaffinity Labeling of S1 with Mant-8-N_3-ADP—30 mM S1 was preincubated with 60 mM Mant-8-N_3-ATP for 20 min at 25°C in buffer comprising 120 mM NaCl, 30 mM Tris-HCl (pH 7.5), and 2 mM $MgCl_2$. After complete hydrolysis of Mant-8-N_3-ATP to Mant-8-N_3-ADP, 1 mM $BeSO_4$, and 5 mM NaF were added and the mixture was incubated for 1 h at 25°C. Untrapped Mant-8-N_3-ADP and BeFn were removed by centrifugal gel filtration on a Sephadex G-50 column equilibrated with 120 mM NaCl and 30 mM Tris-HCl (pH 7.5). The solution containing the isolated complex was then irradiated on ice for 3 min with 366nm UV light (UVL-56 16W, Ultraviolet Products).

Photoaffinity Labeling of S1 with Mant-2-N_3-ADP—30 mM S1 was incubated with 45 mM Mant-2-N_3-ATP as described above for Mant-8-N_3-ATP. After complete hydrolysis to Mant-2-N_3-ADP, 1 mM $BeSO_4$, and 5 mM NaF were added and the mixture was incubated for 30 min at 25°C. Untrapped Mant-2-N_3-ADP and BeFn were then removed and the remaining solution containing the isolated complex was irradiated as described for Mant-8-N_3-ATP.

Quantification of Fluorescent ADP Analog Trapped or Crosslinked to S1—The values of [Mant-2 (or 8)-N_3-ADP] mol/[S1] mol were estimated by comparing the fluorescence intensity of the samples in a buffer of 5 M Guanidine-HCl and 30 mM Tris-HCl (pH 7.5) with the intensity of 30 mM Mant-2 (or 8)-N_3-ATP in the same buffer.

Removal of Noncovalently Bound Mant-2 (or 8) -N_3-ADP and BeFn—Noncovalently bound Mant-2 (or 8)-N_3-ADP and BeFn trapped in the ATP-binding cleft of S1 were removed by adding excess Mg^{2+}ATP and actin as described previously (*8*).

Fluorescence Spectroscopy—Steady-state fluorescence measurements were made with an RF-5000 Spectrofluorophotometer (Shimadzu). Unless otherwise stated, all fluorescence measurements were carried out in buffer containing 120 mM NaCl, 30 mM Tris-HCl pH 7.5, and 2mM $MgCl_2$, at 25°C.

Fluorescence Polarization—Steady-state polarized light was used to excite Mant-S1, and the intensity of the emitted fluorescence was measured at both horizontal (I_h) and vertical (I_v) angles to the incident polarized plane. The excitation wavelength was 360 nm (band width, 5 nm), and fluorescent emission was detected at 445 nm at a band width of 10 nM. Fluorescence polarization (P) was calculated from the following equation.

$$P = (I_h - I_v)/(I_h + I_v)$$

FRET spectroscopy—The efficiency of FRET was calculated from the steady-state emission spectra of Mant fluorescence using the following equation:

$$E = \frac{f_a F_D - \{F_{DA} - (1 - f_a)F_D\}}{f_a F_D}$$

where F_D is the fluorescence intensity of the donor (Mant) in the absence of an acceptor (TNP), F_{DA} is the intensity of the donor in the presence of the acceptor, and f_a is the fraction of acceptor sites occupied by the acceptor. In the present study, $f_a = 1$ was assumed because an excess of P_i analog over Mant-labeled S1 was used. The distance (R) between the donor and acceptor was determined from

$$R = R_0\left(\frac{1}{E} - 1\right)^{\frac{1}{6}}$$

where R_0 is the Forster distance between donor and acceptor probes at which the efficiency is 50%, and is given by

$$R_0^6 = \frac{9 \times 10^{17}(\ln 10)}{128\pi N_A} n^{-4} \kappa J[\mathrm{nm}^6]$$

$$= (8.79 \times 10^{-11}) n^{-4} Q \kappa^2 J[\mathrm{nm}^6]$$

where n is the refractive index of the solution (taken as 1.4), Q is the donor quantum yield (taken as 0.14), κ^2 is the orientation factor (a value of 2/3 was used in the present calculation, assuming that donor and acceptor groups rotate freely in a short time relative to the excited state lifetime of the donor), and J is the overlap integral between the emission spectrum of the donor and the absorption spectrum of the acceptor in units of nm^4 M^{-1} cm^{-1}. The value of J was approximated by the following summation:

$$J = \frac{\Sigma F_D(\lambda)\varepsilon_A(\lambda)\lambda^4 \Delta\lambda}{\Sigma F_D(\lambda)\Delta\lambda}$$

where $\varepsilon_A(\lambda)$ is the extinction coefficient of the acceptor at a given wavelength. The summation was taken over 4 nm intervals.

Acrylamide Quenching—Acrylamide (0–100 mM) quenching of Mant-8 (or 2)-N_3-ADP fluorescence was measured as previously (*12*, *13*). The Stern-Volmer quenching constant (K_{sv}) was calculated from the following equation:

$$F_0/F = 1 + K_{sv}[Q]$$

where F_0 and F are fluorescence intensities in the absence and presence of quencher, respectively, and [Q] is the concentration of acrylamide.

SDS-PAGE—Electrophoresis was performed in 7.5–20% polyacrylamide gradient slab gels in the presence of 0.1%

Downloaded from http://jb.oxfordjournals.org/ at Peking University on October 1, 2012

SDS at a constant voltage (200 V) in the discontinuous buffer system of Laemmli (*14*).

ATPase Assay—ATPase activity was measured at 25°C in a reaction mixture containing 0.5 M KCl, 30 mM Tris-HCl (pH 7.5), 1 mM S1 (or labeled S1), 5 mM $MgCl_2$ ($CaCl_2$ or EDTA), and 2 mM ATP. In the case of actin-activated ATPase, 40 mM KCl, 10 mM Tris-HCl (pH 7.5), 2 mM $MgCl_2$, and 2 mg/ml actin were used. The reaction was stopped by the addition of 10% trichloroacetic acid, and the released Pi was measured by the method of Youngburg and Youngburg (*15*).

RESULTS

Specific Labeling of Loop N with Mant-2-N_3-ADP—Photolabeling of S1 with Mant-2-N_3-ADP was accomplished using the protocol described in "MATERIALS AND METHODS." To reduce nonspecific binding, prior to UV photoirradiation, Mant-2-N_3-ADP was trapped in the ATPase site with BeFn, and the free analogue was removed. Maximal entrapment of Mant-2-N_3-ADP was achieved in the presence of a 1.5-

TABLE I. **Efficiencies of trapping and photolabeling of fluorescent ADP derivatives by BeFn.**

Preparation	Trapped Mant-2-N_3-ADP (mol/mol site)	Labeled Mant-2-N_3-AP (mol/mol site)
1	0.90	0.18
2	0.94	0.20
3	0.87	0.18
Preparation	**Trapped Mant-8-N_3-ADP (mol/mol site)**	**Labeled Mant-8-N_3-AP (mol/mol site)**
1	0.74	0.22
2	0.75	0.24
3	0.76	0.25

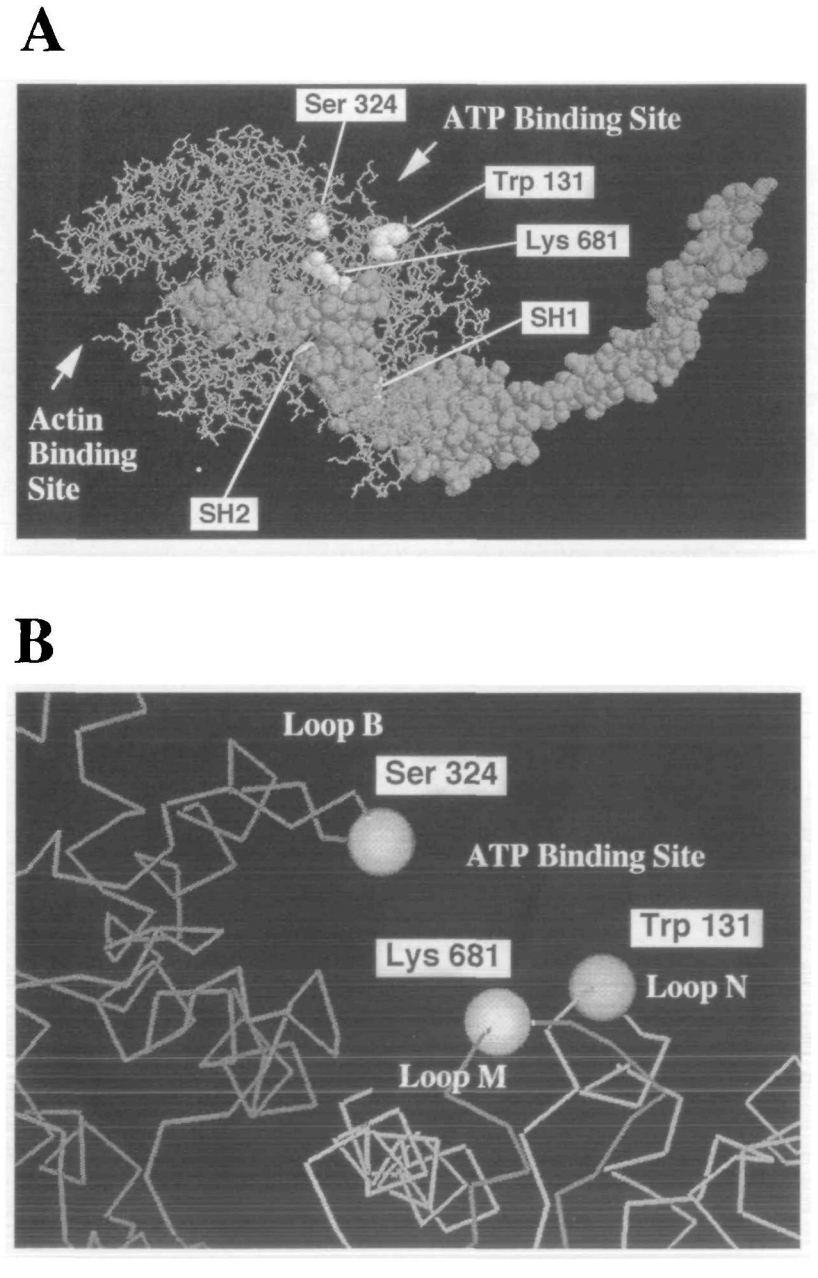

Fig. 1. A: **Space filling representation of the 20 kDa tryptic fragment within the myosin S1 heavy chain ternary structure.** The 25 and 50 kDa fragments are shown as stick representations. Amino acid residues Ser 324 in loop B, Trp 130 in loop N, and Lys 681 in loop M are highlighted, as are the highly reactive cysteine residues of SH1 (707) and SH2 (697). **B: α-carbon chain backbone representation of the ATP-binding cleft of myosin S1.** *Three unique loops*—B, M and N—in the ATP binding site are shown. The α-carbons of Ser 324, Trp 130, and Lys 681 were shown as space filling models. Panels A and B were prepared with the molecular graphic program MacImdad (ver. 5) using the coordinates published by Rayment *et al.* (pdb. 2MYS).

Downloaded from http://jb.oxfordjournals.org/ at Peking University on October 1, 2012

fold molar excess of Mant-2-N_3-ADP (0.9 mol Mant-2-N_3-ADP/mol ATPase site; Table I). Subsequent UV irradiation caused the covalent linkage of Mant-2-N_3-ADP to S1 with an efficiency of 0.2 mol/mol ATPase site. The efficiency of the photoincorporation was lower than the trapping efficiency as a consequence of tetrazole formation: in solution, 2-N_3-ADP readily tautomerizes between the photolabile azido form and two stable tetrazolo isomers (*16*).

It is known that skeletal S1 is photolabeled by 2-N_3-ATP at Trp 130 (*17*), and that a Mant-group bound to the ribose does not affect the capacity of ATP to serve as a substrate for myosin (*18*). Further, crystallographic analysis of the *Dictyostelium* S1-Mant-ADP-BeFn complex showed that the adenine of Mant-ADP coordinates to the site at a similar conformation to that of unmodified ADP (*19*). In the present study, SDS-PAGE analysis of S1 photolabeled with Mant-2-N_3-ADP after mild trypsinization revealed Mant-2-N_3-ADP fluorescence to be present only in the 23 and 25 kDa fragments (Fig. 3B). The 23 kDa fragment was identified as a degradation product of the 25 kDa fragment, as specific antibodies against the latter also recognized the former (*6*). Mild trypsinization after removing uncross-linked Mant-2N_3-ADP from the ATPase site by ATP and actin generated less 23 kDa fragment (Fig. 3B, lanes 3 and 6) than in the case of trypsinization before removing uncross-linked Mant-2N_3-ADP ((Fig. 3B, lanes 2 and 5). These results are consistent with the notion that Trp 130 in loop N is the site that is photolabeled with Mant-2-N_3-ADP. In contrast, as shown in Fig. 3A lane 2, Mant-8-N_3-ADP fluores-

TABLE II. **ATPase activities of S1 photolabeled with Mant-8 (or 2)-N_3-ADP.**

	S1	Mant-2-S1 (Loop N[b])	Mant-8-S1 (Loop M[c])
		(P_i mol/S1 mol/min at 25°C)	
Mg^{2+}-ATPase	0.6	1.2	1.7
Mg^{2+}-ATPase (+actin)[a]	31	34	64
Ca^{2+}-ATPase	62	52	57
EDTA(K^+)-ATPase	150	120	122

[a]2 mg/ml actin. [b]20.0% labeled. [c]22.0% labeled.

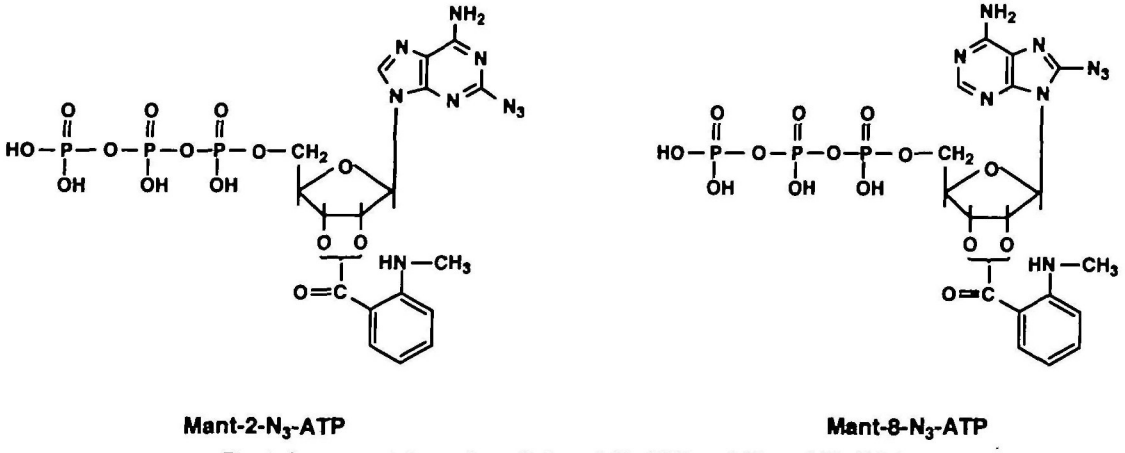

Fig. 2. **Structural formulas of Mant-2-N_3-ADP and Mant-8-N_3-ADP.**

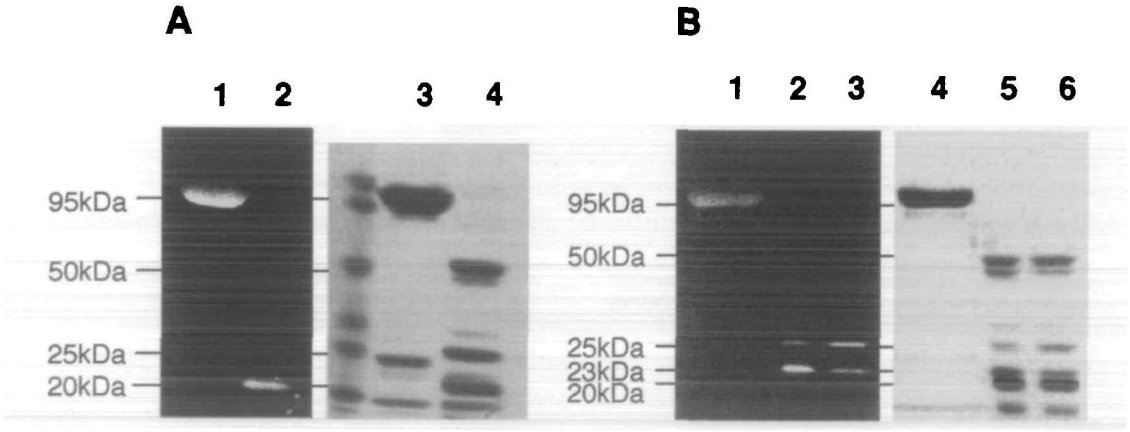

Fig. 3. **Photolabeling of S1 with Mant-8-N_3-ADP or Mant-2-N_3-ADP.** A: S1 was photolabeled with Mant-8-N_3-ADP as described in "MATERIALS AND METHODS" (lanes 1 and 3), then digested with 1/100 (w/w) trypsin for 30 min at 25°C (lanes 2 and 4); lanes 1 and 2, fluorescence of the Mant group crosslinked to S1 or its free tryptic fragment under UV irradiation at 366 nm; lanes 3 and 4, corresponding bands stained with Coomassie Brilliant Blue. B: S1 photolabeled with Mant-2-N_3-ADP, then digested with 1/100 (w/w) trypsin for 30 min at 25°C (lanes 2 and 5); lanes 1, 2, and 3 fluorescence of the Mant group crosslinked to S1 or its tryptic fragment under UV irradiation at 366 nm; lanes 3 and 6, tryptic digests of Mant-S1 after removal of noncovalently bound Mant-2-N_3-ADP and BeFn; lanes 4, 5, and 6, corresponding bands stained with Coomassie Brilliant Blue.

Downloaded from http://jb.oxfordjournals.org/ at Peking University on October 1, 2012

cence was present only in the 20 kDa fragment, which contains loop M.

Enzymatic Activity of S1 Labeled with Mant-2-N_3-ADP—Measurement of the divalent cation-dependent ATPase activity of Mant-2-S1 revealed the EDTA(K^+)-ATPase activity to be reduced by 80%, while the Ca^{2+}-ATPase activity was reduced by 83%, as compared with unlabeled S1 (Table II). In contrast, the Mg^{2+}-ATPase activity of Mant-2-S1 was about 5-fold greater than that of unlabeled S1, and the actin-activated ATPase activity was about 1.5-fold higher than that of unlabeled S1 (Table II). As a control, UV photoirradiation for free S-1 did not affect its activity under these conditions (not shown), suggesting that the change in activity depends on incorporated Mant-2-N_3-ADP. Thus, in the presence of Mg^{2+}, the rate at which Mant-2-S1 hydrolyzes ATP increases apparently, and is not inhibited, even though loop N has been covalently photolabeled with an ADP analogue. When considered in the context of our earlier finding that the ATPase activity of Mant-8-S1 is similar to that of Mant-2-S1 (*6*), these results confirm that the Mg^{2+}-ATPase activity is not blocked by photolabeling S1 with Mant-2 (or 8) -N_3-ADP.

Fluorescence Polarization of Mant-2-S1—The polarization of Mant-group fluorescence was measured in order to

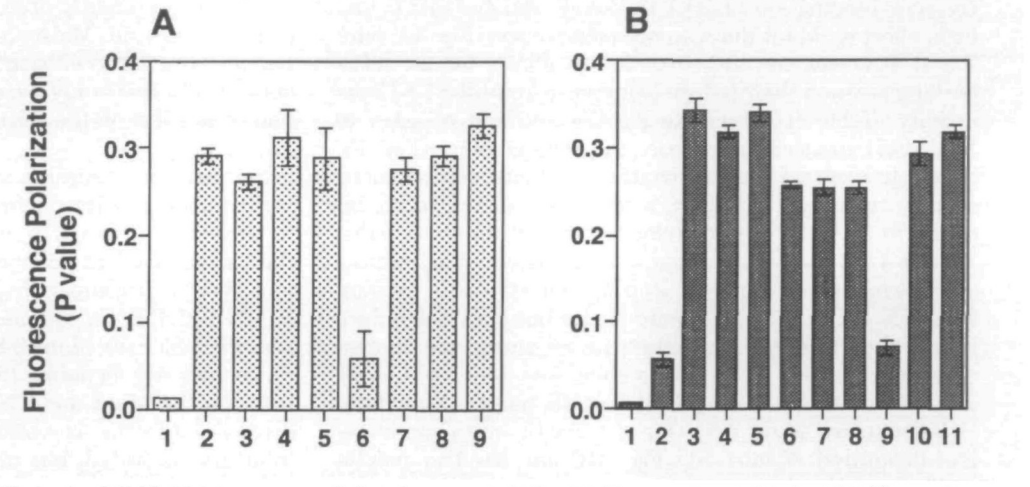

Fig. 4. **Fluorescence emission polarization of Mant-2-N_3-ADP and Mant-8-N_3-ADP derivatives.** A: (1) Free Mant-2-N_3-ATP; (2) 0.5 μM Mant labeled-S1 (Mant-2-S1); (3) 0.5 μM Mant-2-S1 + 2 mM Mg^2'ATP; (4) 0.5 μM Mant-2-S1 + 2.5 mM actin; (5) 0.5 μM Mant-2-S1 + 2 mM Mg^2'ATP and 2.5 μM actin; (6) 0.5 μM Mant-2-S1 + 5M Guanidine-HCl; (7) 0.5 μM Mant-2-S1 + 2 mM Ca^2'ATP; (8) 0.5 μM Mant-2-S1 + 2 mM K'ATP; (9) 0.5 μM Mant-2-S1 + 1 mM BeFn. Samples (1)–(5) and (9) were measured in buffer containing 120 mM NaCl, 30 mM Tris-HCl (pH 7.5) and 2 mM $MgCl_2$; (7) and (8) were measured in buffer containing 0.5M KCl, 30 mM Tris-HCl (pH 7.5) and 2 mM $CaCl_2$ (or 2 mM EDTA). The amount of photoincorporated Mant-2-S1 was estimated to be 18%. The excitation and emission wavelengths were 360 and 445 nm, respectively. The error bars represent the maximum deviation from the mean values of three to five experiments. B: (1) Free Mant-8-N_3-ATP; (2) Mant-8-N_3-ATP + 0.25 μM actin; (3) S1·Mant-8-N_3-ADP·BeFn complex; (4) 0.5 μM Mant labeled-S1(Mant-8-S1); (5) 0.5 μM Mant-8-S1 + 1mM BeFn; (6) 0.5 μM Mant-8-S1 + 2 mM Mg^2'ATP; (7) 0.5 μM Mant-8-S1 + 2.5 μM actin; (8) 0.5 μM Mant-8-S1 + 2 mM Mg^2'ATP and 2.5 μM actin; (9) 0.5 μM Mant-8-S1 + 5 M Guanidine-HCl; (10) 0.5 μM Mant-8-S1 + 2 mM Ca^2'ATP; (11) 0.5 μM Mant-8-S1+ 2 mM K'ATP. Samples (1)–(8) were measured in buffer containing 120 mM NaCl, 30 mM Tris-HCl pH 7.5, and 2 mM $MgCl_2$; (10) and (11) were measured in buffer containing 0.5 M KCl, 30 mM Tris-HCl (pH 7.5) and 2 mM $CaCl_2$ (or 2 mM EDTA). The amount of photoincorporated Mant-8-S1 was estimated to be 22%. The data shown in panel B are taken from our previous report (*6*).

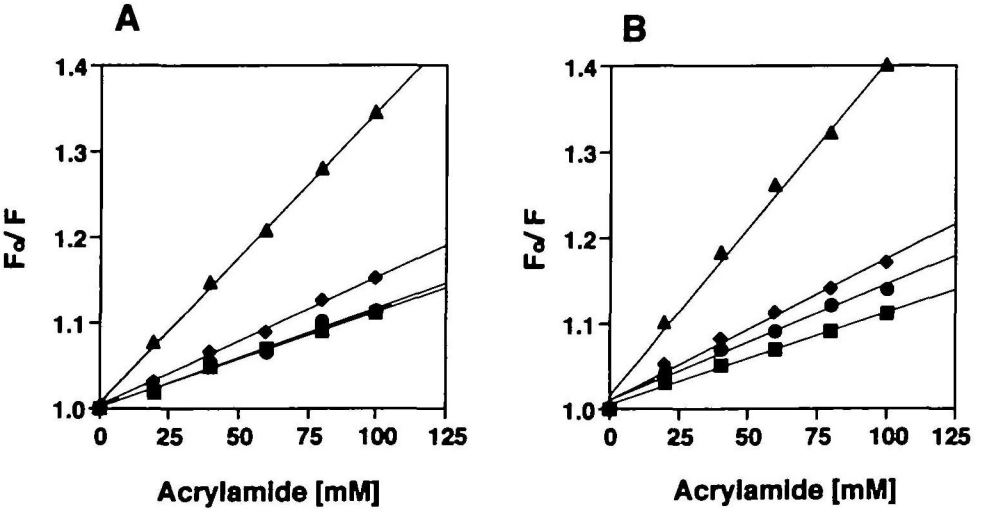

Fig. 5. **Stern-Volmer plots of acrylamide quenching of the fluorescence of Mant-2-N_3-ADP and Mant-8-N_3-ADP derivatives.** A: Free Mant-2-N_3-ATP in solution (▲); 0.5 μM Mant-2-S1 (■); 0.5 μM Mant-2-S1 + 2 mM Mg^2'ATP (◆); 0.5 μM Mant-2-S1 + 5 μM actin (●). The amount of photoincorporated Mant-2-S1 was estimated to be 18%. B: Free Mant-8-N_3-ATP in solution (▲); 0.5 μM Mant-8-S1 (■); 0.5 μM Mant-8-S1 + 2 mM Mg^2'ATP (◆); 0.5 μM Mant-8-S1 + 5 μM actin (●). The amount of photoincorporated Mant-8-S1 was estimated to be 22%. The data shown in panel B are taken from our previous report (*1*). All experiments were performed using buffer containing 120 mM NaCl, 30 mM Tris-HCl pH 7.5, and 2 mM $MgCl_2$. The amount of photo-incorporation of the Mant group into S1 was estimated from the fluorescence intensities in 5 M Guanidine-HCl and 30 mM Tris-HCl (pH 7.5), as described in "MATERIALS AND METHODS." The excitation and emission wavelength were 360 and 445 nm, respectively.

Downloaded from http://jb.oxfordjournals.org/ at Peking University on October 1, 2012

observe the effects of Mg^{2+}-ATP and actin on the mobility of Mant-2-N_3-ADP cross-linked to loop N. The fluorescence polarization of Mant-2-S1 was compared with the results of Mant-8-S1 reported previously (*6*) (Fig. 4B). Cross-linking Mant-2-N_3-ADP to S1 significantly increased the polarization (Fig. 4A, bar 2), and the subsequent addition of 1 mM BeFn increased it somewhat further (Fig. 4A, bar 9); similar responses were seen with Mant-8-S1 (Fig. 4B, bars 4 and 5). Mg^{2+}ATP diminished Mant-2-S1polarization (Fig. 4A, bar 3), presumably by the same mechanism responsible for diminishing Mant-8-S1 polarization (Fig. 4B, bar 6). The increased probe mobility is consistent with Mg^{2+}-ATP competitively displacing Mant-2-N_3-ADP or Mant-8-N_3-ADP from the ATP-binding site to a less hindered site outside the ATP-binding site. EDTA (K^+)-ATP and Ca^{2+}-ATP had little effect on Mant fluorescence polarization (Fig. 4A, bars 7 and 8), consistent with their lower affinity for the ATP-binding site and their failure to increase Mant-2-S1 ATPase activity (Table II). Interestingly, the addition of actin to Mant-8-S1 induced an increase in probe mobility (Fig. 4B, bar 7). In contrast, the polarization of Mant-2-S1 increased slightly upon actin binding, which may be due to an increase in the rotational correlation time of Mant-2-S1 (Fig. 4A, bar 4). These results suggest that actin binding induces a conformational change at loop M that results in moving Man-8-N_3-ADP to a less hindered site but does not induce loop N significantly. As a control, we measured the fluorescence polarization of highly mobile free Mant-2-N_3-ADP (Fig. 4A bar 1), Mant-8-N_3-ADP (Fig. 4B, bar 1), Guanidine-HCl-denatured Mant-2-S1 (Fig. 4A bar 6), and Guanidine-HCl-denatured Mant-8-S1 (Fig. 4B, bar 9). The results showed very low polarization confirming that the polarization measurements reflect the mobility of the Mant-group.

Acrylamide Quenching of Mant-2-S1 Fluorescence—If Mant-2-N_3-ADP or Mant-8-N_3-ADP is displaced from the ATP-binding site cleft by Mg^{2+}-ATP and/or actin, the fluorescent Mant-group should then be more accessible to the ambient solution and to dissolved quenching compounds such as acrylamide. To show this, Mant-S1 fluorescence was measured under conditions identical to those described in Fig. 4. As a control, the value of K_{sv} for free Mant-2-N_3-ADP and Mant-8-N_3-ADP in solution were calculated to be 3.41 M^{-1} (Fig. 5A, triangles) and 3.90 M^{-1} (Fig. 5B, triangles), respectively. The value of Mant-2-S1 and Mant-8-S1 were 1.13 M^{-1} (Fig. 5A, squares) and 1.07 M^{-1} (Fig. 5B, squares), respectively. The lower quench constants for Mant-S1s illustrate that Mant-2-N_3-ADP and Mant-8-N_3-ADP were relatively inaccessible to dissolved acrylamide when bound inside the ATP binding cleft. In the presence of ATP, the values for Mant-2-S1 and Mant-8-S1 increased to 1.51 M^{-1} (Fig. 5A, diamonds) and 1.64 M^{-1} (Fig. 5B, diamonds), respectively. These results are consistent with the increased rotational mobility of the probe (Fig. 4). For Mant-2-S1, actin-binding had little effect on the K_{sv} (1.17 M^{-1}) (Fig. 5A, circles). These findings are consistent with the results of the polarization experiments and further confirm that actin binding does not induce significant conformational changes in loop N. In contrast, actin binding increased the value of K_{sv} for Mant-8-S1 (Fig. 5B), indicating that actin binding does indeed induce a conformational change in loop M.

FRET between the Mant-Group on Unique Loops in the ATPase Site—The overlap of the fluorescence spectra of Mant-2-N_3-ATP and Mant-8-N_3-ATP with the absorption spectrum of TNP-ATP makes in possible for FRET to occur between them (Fig. 6). From the overlapped spectra, the value of J, which was the same for Mant-2-N_3-ATP and Mant-8-N_3-ATP, was calculated to be 7.21×10^{14} [nm^4 M^{-1} cm^{-1}], yielding an Ro of 34.0 Å (see "MATERIALS AND METHODS" for the calculation). The absorption spectrum of TNP-ADP changes slightly after binding to S1 due to the disappearance of the Meisenheimer complex; nonetheless, a molar extinction coefficient of 26,400 M^{-1} cm^{-1} at 408 nm was used in this study, because the change in the spectrum had little effect on the calculation of R_0 (less than 1 Å; data not shown).

Because the emission spectrum of Mant fluorescence shifted slightly after photolabeling S1, R_0 was recalculated in each case (Table III). As a preliminary study of FRET, the time-dependent changes in Mant-8-S1 fluorescence intensity that accompanying the formation of the Mant-8-S1·TNP-ADP·BeFn complex were observed. Addition of 2.5 μM TNP-ATP to Mant-8-S1 greatly reduced the fluorescence intensity, signaling that a transfer of energy occurred between the Mant and TNP groups (Fig. 7, A and B, first arrow). After the complete hydrolysis of TNP-ATP, the intensity recovered, but did not return completely to the level seen before its addition. This incomplete recovery is

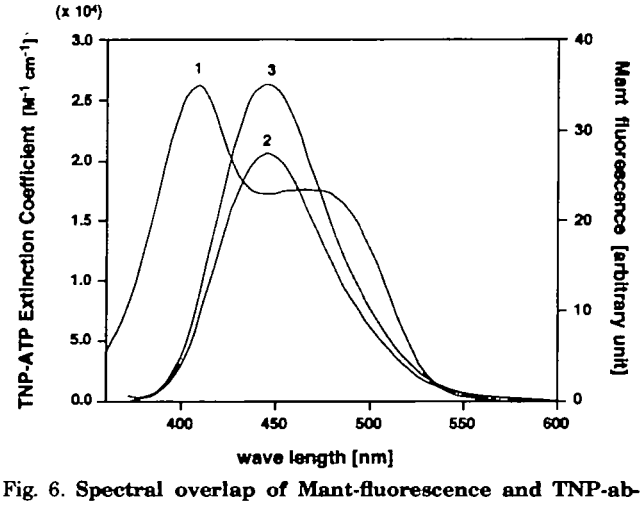

Fig. 6. **Spectral overlap of Mant-fluorescence and TNP-absorption.** Plotted are the absorption spectrum of TNP-ATP (fluorescence acceptor; curve 1) and the fluorescence emission spectra of Mant-2-N_3-ATP (curve 2) and Mant-8-N_3-ATP (curve 3) in arbitrary units. The emission spectra gave the same value for *J*, 7.21×10^{14} [nm^4 M^{-1} cm^{-1}], which yielded an R_0 of 34.0 Å, assuming $k^2 = 2/3$.

TABLE III. **Summary of FRET measurements.**

Species	R_0 (Å)	Efficiency (%) [mean ± SD (*n*)]	Distance (Å) [mean ± SD (*n*)]
Mant-8-S1·TNP-ADP·BeFn	33.5	47.6 ± 5.0 (3)	34.0 ± 1.2 (3)
Mant-8-S1·TNP-ADP·AlF_4^-	33.3	64.0 ± 4.6 (3)	30.2 ± 1.0 (3)
Mant-2-S1·TNP-ADP·BeFn	33.4	51.2 ± 3.2 (3)	33.1 ± 0.7 (3)
Mant-2-S1·TNP-ADP·AlF_4^-	33.1	50.8 ± 2.3 (3)	32.9 ± 0.5 (3)

Downloaded from http://jb.oxfordjournals.org/ at Peking University on October 1, 2012

consistent with a previously described inner filter effect of TNP-ADP and with non-specific binding of TNP-ADP to S1, which likely causes additional FRETs (*20, 21*). For Mant-2-S1, the recovery of Mant-2-S1 fluorescence intensity following hydrolysis of TNP-ATP was even less complete than that seen with Mant-8-S1. This implies even greater nonspecific binding of TNP-ADP, causing the occurrence of other FRETs (Fig. 7, C and D, first arrow). The subsequent addition of 2 mM BeFn reduced the fluorescence intensity to a level comparable to that seen with TNP-ATP, signaling formation of Mant-8-S1·TNP-ADP·BeFn and Mant-2-S1·TNP-ADP·BeFn ternary complexes (Fig. 7, A and C, second arrow). An additional 1mM BeFn (3 mM final concentration) had no effect on the intensity, indicating that 2 mM BeFn was sufficient to saturate the ATPase sites with TNP-ADP·BeFn (Fig. 7, A and C, third arrow). The addition of 2 mM AlF_4^- elicited greater declines in Mant-8-S1 fluorescence intensity than did BeFn (Fig. 7B, second arrow), and the subsequent addition of 1 mM AlF_4^- (3 mM final concentration) did not change the intensity, suggesting that 2 mM AlF_4^- is sufficient to saturate the ATPase site with TNP-ADP/AlF_4^- (Fig. 7B, third arrow). The difference in fluorescence intensity between the Mant-8-S1·TNP-ADP·BeFn and Mant-8-S1·TNP-ADP·AlF_4^- complexes may reflect a difference in the distance between the TNP-group in the ATPase site and Mant-group on loop M in the two complexes. As it is believed that M·ADP·AlF_4^- mimics the M^{**}·ADP·P_i state and M·ADP·BeFn mimics the M^*·ATP state, this finding suggests that loop M changes its conformation during the ATPase cycle. On the contrary, the addition of BeFn or AlF_4^- to the Mant-2-S1 solution containing TNP-ADP reduced the fluorescence intensity to about the same degree (Fig. 7, C and D), indicating that the distance between loop N and the ATPase site remains about the same throughout the ATPase cycle.

To calculate the distance between loop M or loop N and the active site, more precisely the Mant fluorescence emission spectra were compared and the efficiencies of energy transfer were determined (Fig. 8, A and B). To compensate for the inner filter effect and the nonspecific binding of TNP-ATP, its binding to the ATPase site was blocked in control samples by preincubating Mant-8-S1 or Mant-2-S1 with ADP and BeFn (or AlF_4^-), and then the same concentration of TNP-ATP (10 μM) was added (Fig. 8, A and B, curves 1 and 2). For Mant-8-S1, the values of J determined using curves 1 and 2 in Fig. 8A as donor spectra were 7.02 × 10^{14} [nm^4 M^{-1} cm^{-1}] and 7.01 × 10^{14} [nm^4 M^{-1} cm^{-1}], respectively, yielding R_0s of 33.5 and 33.3 Å. The calculated energy transfer efficiencies were 47.6% for the Mant-8-S1·TNP-ADP·BeFn complex and 64.0% for the Mant-8-S1·TNP-ADP·AlF_4^- complex, which puts the distance between loop M and the active site in the two complexes at 34.0 and

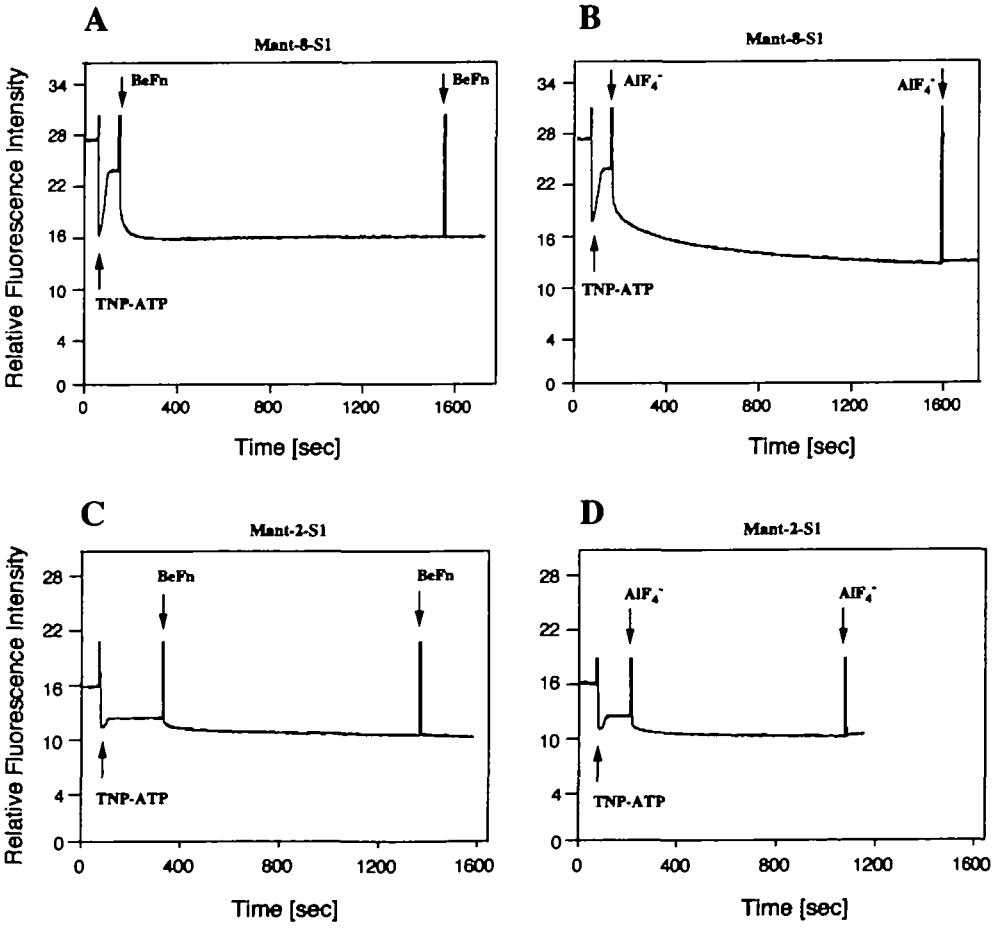

Fig. 7. **Time-course of fluorescence emission intensity of S1 labeled at loop M with Mant-8-N_3-ADP and S1 labeled at loop N with Mant-2-N_3-ADP.** A: Arrowheads indicate the successive addition of 2.5 μM TNP-ATP, 2 mM BeFn, and 1 mM BeFn (3 mM total) to 0.25 μM Mant-8-S1. The amount of photoincorporated Mant-8-S1 was estimated to be 22%. B: Arrowheads indicate the successive addition of 2.5 μM TNP-ATP, 2 mM AlF_4^-, and 1 mM AlF_4^- (3 mM total) to 0.25 μM Mant-8-S1. The amount of photoincorporated Mant-8-S1 was estimated to be 22%. C: Arrowheads indicate the successive addition of 2.5 μM TNP-ATP, 1 mM BeFn, and 1 mM BeFn (2 mM total) to 0.25 μM Mant-2-S1. The amount of photoincorporated Mant-2-S1 was estimated to be 18%. D: Arrowheads indicate the successive addition of 2.5 μM TNP-ATP, 1 mM AlF_4^- and 1 mM AlF_4^- (2 mM total) to 0.25 μM Mant-2-S1. The amount of photoincorporated Mant-2-S1 was estimated to be 18%. Measurements shown in A and B were made in buffer containing 120 mM NaCl, 30 mM Tris-HCl pH 7.5, and 2 mM $MgCl_2$ at 25°C. The excitation and emission wavelengths were 360 and 445 nm, respectively.

Downloaded from http://jb.oxfordjournals.org/ at Peking University on October 1, 2012

30.2 Å, respectively (Table III). For Mant-2-S1, the values of J, determined using curves 1 and 2 in Fig. 8B as donor spectra, were 6.94×10^{14} [nm^4 M^{-1} cm^{-1}] and 7.01×10^{14} [nm^4 M^{-1} cm^{-1}], respectively, yielding R_0s of 33.4 and 33.1 Å. The calculated energy transfer efficiencies were 51.2% for Mant-2-S1·TNP-ADP·BeFn complex and 50.8% for Mant-2-S1·TNP-ADP·AlF_4^- complex, which put the distances between loop N and the active site in the two complexes at 33.1 and 32.9 Å, respectively.

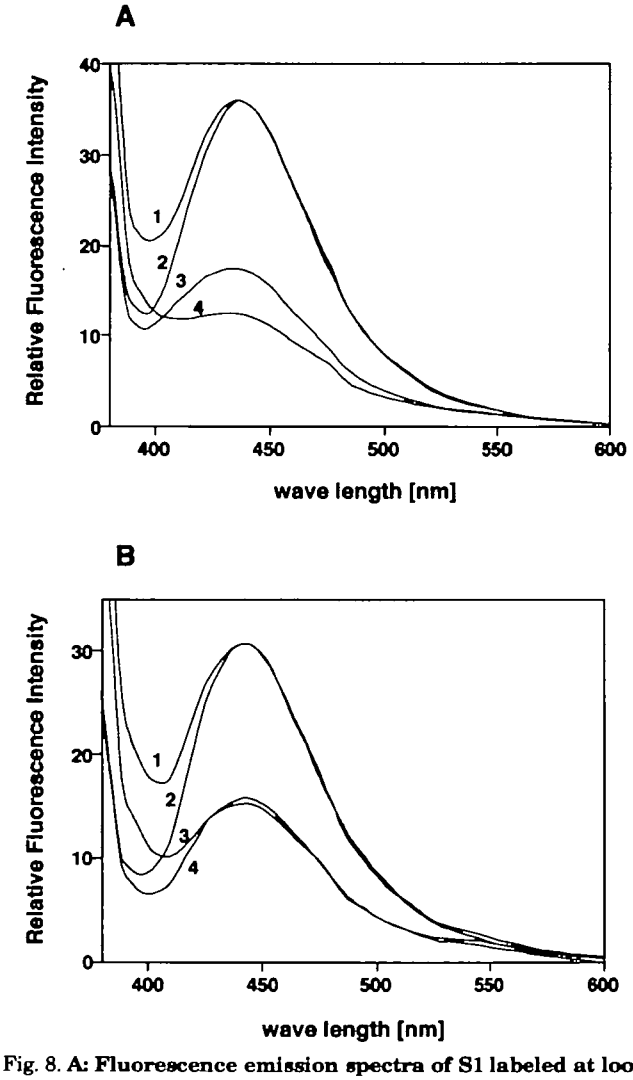

Fig. 8. **A: Fluorescence emission spectra of S1 labeled at loop M with Mant-8-N_3-ADP.** (1) 0.25 μM Mant-8-S1 in the presence of 0.5 mM ADP, 2 mM AlF_4^- and 10 μM TNP-ATP (added last); (2) 0.25 μM Mant-8-S1 in the presence of 0.5 mM ADP, 2 mM BeFn, and 10 μM TNP-ATP (added last); (3) 0.25 μM Mant-8-S1 in the presence of 10 μM TNP-ADP and 2 mM BeFn; (4) 0.25 μM Mant-8-S1 in the presence of 10 μM TNP-ADP and 2 mM AlF_4^-. **B: Fluorescence emission spectrum of S1 labeled at loop N with Mant-2-N_3-ADP.** (1) 0.25 μM Mant-2-S1 in the presence of 0.5 mM ADP, 1 mM AlF_4^- and 10 μM TNP-ATP (added last); (2) 0.25 μM Mant-2-S1 in the presence of 0.5 mM ADP, 1 mM BeFn, and 10 μM TNP-ATP (added last); (3) 0.25 μM Mant-2-S1 in the presence of 10 μM TNP-ADP and 1 mM AlF_4^-; (4) 0.25 μM Mant-2-S1 in the presence of 10 μM TNP-ADP and 1 mM BeFn. The amount of photoincorporated Mant-2-S1 was estimated to be 20%. Other conditions were the same as given for Figs. 7 and 8. The data shown are representative of those from three independently prepared samples.

DISCUSSION

The aim of the present study was to clarify further the functions of unique loops near the ATP binding cleft; we hypothesize that their functions are directly related to energy transduction. We have employed specific photoaffinity labeling at the loops using fluorescence labeled ADP analogues to monitor conformational changes at the loops.

Several photoaffinity labeling ATP analogues that crosslink to the unique loops have been used to study the myosin ATPase site (*17*, *22–24*). In particular, Grammer *et al.* (*17*) identified the amino acid residue labeled by 2-N_3-ADP to be 130 Trp. This is consistent with the crystallographic structures of smooth muscle, scallop and *Dictyostelium* muscle myosin-ADP-fluorometal ternary complexes, which show that the adenine ring faces a group of amino acids that includes 130 Trp (*3*, *4*, *25*). In this context, the fact that Mant-ADP trapped by BeFn into *Dictyostelium* S1 coordinates similarly to unmodified ADP (*19*), and that only the 25 kDa fragment and its 23 kDa degradation product showed Mant fluorescence following photoirradiation (Fig. 3B, lanes 2 and 3), makes it likely that Mant-2-N_3-ADP crosslinks to 130 Trp in loop N.

Due to steric hindrance, in solution, ATP analogues with bulky groups at the eighth position of the adenine ring, including 8-N_3-ATP, predominantly assume the *syn* conformation with respect to the *N*-glycoside bond and do not induce actin sliding with skeletal S-1 (*26–28*). It is suggested that a modified adenine moiety is almost certainly not bound to the intrinsic adenine binding site. Mant-8-N_3-ADP is trapped by BeFn into the ATPase site of SKE-S1. The 3D structure of SKE-S1 shows that only loop M, Lys 681 in particular, protrudes into the ATP binding cleft, and because of the lengths of Mant-8-N_3-ADP and the side chain of Lys 681 protruding into the ATP-binding cleft, Lys 681 should be able to react with the entrapped Mant-8-N_3-ADP. Indeed, complete digestion of the Mant-8-N_3-ADP-labeled, 20-kDa fragment by lysyl-endopeptidase yields the peptide Leu 660–Lys 702, containing Lys 681 (*5*). Moreover, the photoaffinity-labeling ATP analogue SSL-NANDP, which carries a bulky spin probe at a position identical to the ribose of normal ATP, crosslinks to Lys 681 (*29*); molecular modeling and dynamics simulations showed that the nitrophenyl ring of SSL-NANDP does not bind in the purine binding site, but rather is tilted towards Lys-681, positioning the photoreactive azido group adjacent to the lysine side-chain (*30*). Thus, the available evidence makes it highly likely that Mant-8-N_3-ADP binds to Lys 681.

When linked to the ribose ring of ATP, the Mant-group does not affect the capacity of ATP to serve as a substrate for myosin (*18*). In the present study, we found that photolabeling loop M with Mant-8-N_3-ADP or loop N with Mant-2-N_3-ADP did not antagonize the hydrolysis of Mg^{2+}ATP or actin binding (Table II), and demonstrated that it is possible to use the specificity of photoaffinity fluorescent analogues to place reporter groups at the unique loops. Fluorescence polarization and acrylamide quenching studies of the fluorescent reporter group at the loops clearly reflected the conformational changes at the loops induced by actin and nucleotide binding. Interestingly, the binding of actin to Mant-8-S1 also significantly decreased the polarization of Mant, but did not affect significantly the polarization of

Downloaded from http://jb.oxfordjournals.org/ at Peking University on October 1, 2012

Mant-2-S1. This suggests that the binding of actin to the actin-binding site, which is situated opposite the ATP-binding site, induces a conformational change in loop M but not in loop N.

To detect conformational changes in the loops during the ATPase cycle, TNP-ADP·BeFn and TNP-ADP·AlF_4^- were employed as FRET acceptors of Mant-fluorescence. The fluorescence intensity of the Mant-group was reduced by the binding of TNP-ATP, signaling the FRET between the TNP-group within the ATP-binding site and Mant-groups on the loops. After complete hydrolysis of TNP-ATP, the fluorescence intensity did not return to its initial level due to the inner filter effect and to nonspecific binding of TNP-ADP, which likely caused other FRETs (*20*, *21*). The inner filter effect alone can be easily corrected for using the equation: $F_{corr} = F_{obs} \times 10\ (A_{ex} + A_{em})/2$, where A_{ex} and A_{em} are the absorptions of the samples at the excitation and emission wavelengths, respectively. But since there was also nonspecific TNP-ADP binding, which can not be estimated precisely, these unfavorable effects were subtracted by using control samples to which the same concentration of TNP-ATP was added only after the formation of Mant-8 (or 2)-S1·Mg^{2+}ADP·BeFn (or AlF_4^-).

Despite the fact that the observed energy transfer efficiencies contained uncertainties due to other FRETs between the Mant-group and TNP-groups at other sites on S1, a single donor-acceptor pair was assumed in our of analysis of FRET. This is because the transfer efficiency varies as function of the sixth power of the distance between the donor and the acceptor; if one acceptor is situated relatively close to a donor and other acceptors lie at somewhat greater distances, the overall transfer efficiency will depend strongly on the distance of the closest acceptor. When two or three acceptors lie equidistant from a single donor, the distance between the donor and the acceptors differs by only 12 or 20%, respectively, from the value calculated for a single donor-acceptor pair (*31*). Consequently, we are confident that the distances between the ATPase site and each loop were calculated without large errors.

That photolabeling S1 with Mant-2-N_3-ADP or Mant-8-N_3-ADP was achieved by trapping with BeFn means there is a possibility that errors were introduced into the data from FRET experiments by retrapping the probe with BeFn. We tested this possibility by assessing the effect of Mg^{2+}ATP or BeFn on the fluorescence emission spectra of Mant-8-S1 and Mant-2-S1. The addition of Mg^{2+}ATP to Mant-8-S1 and Mant-2-S1 caused red spectral shifts of the emission spectra to 436 and 443 nm, respectively. On the other hand, the addition of BeFn in the absence of TNP-ADP or ADP caused blue spectral shifts to 433 and 440 nm, respectively, and the fluorescence intensities were slightly increased in each case. The fluorescence emission spectra used for FRET calculations (Fig. 8) had maximum peaks at 436 nm for Mant-8-S1·TNP-ADP·BeFn and 444 nm for Mant-2-S1·TNP-ADP·BeFn, providing indirect evidence that the ATP-binding site was saturated with TNP-ADP·BeFn, rather than with retrapped Mant-ADP BeFn.

The findings discussed so far reveal the unique role of the 20 kDa tryptic fragment as a signal transducer in the myosin head. In particular, loop M appears to serve as a sensor that signals the actin-binding site of ATP-binding and *vice versa*, and signals the hinge region of the myosin head of ATP-hydrolysis, which may cause a global bending of the myosin head. Earlier studies demonstrating that the modification of SH1 and/or SH2 affects both the ATPase activity and actin binding support this idea (*32*, *33*).

We also hypothesize that signals are transmitted through the long helix. For example, Ho and Chisholm (*34*) recently showed that in *Dictyostelium*, mutation of the myosin essential light chain bound to the helix tail of the myosin head leads to reduced actin-activated ATPase activity, despite stoichiometric binding to the myosin heavy chain. This suggests that signals are transmitted along the backbone helix of the 20 kDa fragment *via* loop M. Interestingly, the loops may also have other functions in other proteins. For example, cooperative swinging of the paired loops of the mitochondrial ADP/ATP carrier appears to mediate the protein's transport function (*35*). A similar loop structure may also be involved in ion channel function in colicin Ia (*36*).

REFERENCES

1. Kull, F.J., Sablin, E.P., Lau, R., Fletterick, R.J., and Vale, R.D. (1996) Crystal structure of the kinesin motor domain reveals a structural similarity to myosin. *Nature* **380**, 550–555
2. Rayment, I., Rypniewski, W.R., Schmidt-Base, K., Smith, R., Tomchick, D.R., Benning, M.M., Winkelmann, D.A., Wesenberg, G., and Holden, H.M. (1993) Three-dimensional structure of myosin subfragment-1: a molecular motor. *Science* **261**, 50–58
3. Fischer, A.J., Smith, C.A., Thoden, J.B., Smith, R., Sutoh, K., Holden, H.M., and Rayment, I. (1995) X-ray structures of the myosin motor domain of *Dictyostelium discoideum* complexed with MgADP.BeFx and MgADP.AlF_4^-. *Biochemistry* **34**, 8960–8972
4. Dominguez, R., Freyzon, Y., Trybus, K.M., and Cohen, C. (1998) Crystal structure of a vertebrate smooth muscle myosin motor domain and its complex with the essential light chain: visualization of the pre-power stroke state. *Cell* **94**, 559–571
5. Maruta, S., Miyanishi, T., and Matsuda, G. (1989) Localization of the ATP-binding site in the 23-kDa and 20-kDa regions of the heavy chain of the skeletal muscle myosin head. *Eur. J. Biochem.* **184**, 213–221
6. Maruta, S. and Homma, K. (1998) A unique loop contributing to the structure of the ATP-binding cleft of skeletal muscle myosin communicates with the actin-binding site. *J. Biochem.* **124**, 528–533
7. Maruta, S., Saitoh, J., and Asakura, T. (2000) Analysis of conformational changes at the unique loop adjacent to the ATP binding site of smooth muscle myosin using a fluorescent probe. *J. Biochem.* **127**, 199–204
8. Luo, Y., Wang, D., Cremo, C.R., Pate, E., Cooke, R., and Yount, R.G. (1995) Photoaffinity ADP analogs as covalently attached reporter groups of the active site of myosin subfragment 1. *Biochemistry* **34**, 1978–1987
9. Perry, S.V. (1952) Myosin adenosine triphosphatase. *Methods Enzymol.* **2**, 582–588
10. Weeds, A.G., and Taylor, R.S. (1975) Separation of subfragment-1 isoenzymes from rabbit skeletal muscle myosin. *Nature* **257**, 54–56
11. Pardee, J.D. and Spudich, J.A. (1982) Purification of muscle actin. *Methods Enzymol.* **85**, 164–168
12. Stern, O. and Volmer, M. (1919) Über die abklingungszeit der fluoreszenz. *Phys. Z.* **20**, 183
13. Lehrer, S.S. and Leavis, P.C. (1978) Solution quenching of protein fluorescence. *Methods Enzymol.* **49**, 222
14. Laemmli, U.K. (1970) Cleavage of structural proteins during the assembly of the head of bacteriophage T4. *Nature* **227**, 680–685
15. Youngburg G.E. and Youngburg, M.V. (1930) A system of blood phosphorus analysis. *J. Lab. Clin. Med.* **16**, 158–166
16. Macfarlane, D.E. and Srivastava, P.C. (1982) Binding of 2-azi-

Downloaded from http://jb.oxfordjournals.org/ at Peking University on October 1, 2012

doadenosine [beta-^{32}P] diphosphate to the receptor on intact human blood platelets which inhibits adenylate cyclase. *Biochemistry* **21**, 544–549
17. Grammer, J.C., Kuwayama, H., and Yount, R.G. (1993) Photoaffinity labeling of skeletal myosin with 2-azidoadenosine triphosphate. *Biochemistry* **32**, 5725–5732
18. Hiratsuka, T. (1983) New fluorescent analogs of adenine and guanine nucleotides available as substrates for various enzymes. *Biochim. Biophys. Acta* **742**, 496–508
19. Bauer, C.B., Kuhlman, P.A., Bagshaw, C.R., and Rayment, I. (1997) X-ray crystal structure and solution fluorescence characterization of Mg·2′(3′)-*O*-(*N*-methylanthraniloyl) nucleotides bound to the *Dictyostelium discoideum* myosin motor domain. *J. Biol. Chem.* **274**, 394–407
20. Tao, T. and Lamkin, M. (1981) Excitation energy transfer studies on the proximity between SH1 and the adenosinetriphosphatase site in myosin subfragment 1. *Biochemistry* **20**, 5051–5055
21. Moss, D.J., Trentham, D.R. (1983) Distance measurement between the active site and cysteine-177 of the alkali one light chain of subfragment 1 from rabbit skeletal muscle. *Biochemistry* **22**, 5261–5270
22. Mahmood, R., Elzinga, M., and Yount, R.G. (1989) Serine-324 of myosin's heavy chain is photoaffinity-labeled by 3′(2′)-*O*-(4-benzoylbenzoyl)adenosine triphosphate. *Biochemistry* **28**, 3989–3995
23. Kerwin, B.A. and Yount, R.G. (1992) Photoaffinity labeling of scallop myosin with 2-[(4-azido-2-nitrophenyl)amino]ethyl diphosphate: identification of an active site arginine analogous to tryptophan-130 in skeletal muscle myosin. *Bioconjug. Chem.* **3**, 328–336
24. Okamoto, Y. and Yount, R.G. (1985) Identification of an active site peptide of skeletal myosin after photoaffinity labeling with *N*-(4-azido-2-nitrophenyl)-2-aminoethyl diphosphate. *Proc. Natl. Acad. Sci. USA* **82**, 1575–1579
25. Houdusse, A., Kalabokis, V.N., Himmel, D., Szent-Gyorgyi, A.G., and Cohen, C. (1999) Atomic structure of scallop myosin subfragment S1 complexed with MgADP: a novel conformation of the myosin head. *Cell* **97**, 459–470
26. Takenaka, H., Ikehara, M., and Tonomura, Y. (1976) Structure and function of the two heads of the myosin molecule. IV. Physiological functions of various reaction intermediates in myosin adenosine triphosphate, studied by the interaction between actomyosin and 8-bromoadenosine triphosphate. *J. Biochem.* **80**, 1381–1392
27. Takeneka, T., Ikehara, M., and Tonomura, Y. (1978) Interaction between actomyosin and 8-substituted ATP analogs. *Proc. Natl. Acad. Sci. USA* **75** 4229–4233
28. Maruta, S., Ohki, T., Kambara, T., and Ikebe, M. (1998) Characterization of the interaction of myosin with ATP analogues having the *syn* conformation with respect to the adenine-ribose bond. *Eur. J. Biochem.* **256**, 229–237
29. Chen, X., Siems, W.F., Asbury, G.R., and Yount, R.G. (1999) Fingerprint patterns from laser-induced azido photochemistry of spin-labeled photoaffinity ATP analogs in matrix-assisted laser desorption/ionization mass spectrometry. *J. Am. Soc. Mass Spectrom.* **10**, 1337–1340
30. Lawson, J.D., Pate, E., Chen, X., Cook, R., and Yount, R.G. (2000) Binding of the SSL-NANDP photoaffinity/spin probe in myosin. *Biophys. J.* **78**, 246a
31. Miki, M., Kobayashi, T., Kimura, H., Hagiwara, A., Hai, H., and Maeda, Y. (1998) Ca^{2+}-induced distance change between points on actin and troponin in skeletal muscle thin filaments estimated by fluorescence energy transfer spectroscopy. *J. Biochem.* **123**, 324–331
32. Mulhern, S.A. and Eisenberg, E. (1978) Interaction of spin-labeled and *N*-(iodacetylaminoethyl)-5-naphthylamine-1-sulfonic acid SH1-blocked heavy meromyosin and myosin with actin and adenosine triphosphate. *Biochemistry* **17**, 4419–4425
33. Reisler, E. (1982) Sulfhydryl modification and labeling of myosin. *Methods Enzymol.* **85**, 84–93
34. Ho, G. and Chisholm, R.L. (1997) Substitution mutations in the myosin essential light chain lead to reduced actin-activated ATPase activity despite stoichiometric binding to the heavy chain. *J. Biol. Chem.* **272**, 4522–4527
35. Majima, E., Shinohara, Y., Yamaguchi, N., Hong, Y.M., and Terada, H. (1994) Importance of loops of mitochondrial ADP/ATP carrier for its transport activity deduced from reactivities of its cysteine residues with the sulfhydryl reagent eosin-5-maleimide. *Biochemistry* **33**, 9530–9536
36. Simon, S. (1994) Ion channels. Enter the 'swinging gate'. *Nature* **371**, 103–104

Downloaded from http://jb.oxfordjournals.org/ at Peking University on October 1, 2012